An *Arabidopsis thaliana* leucine-rich repeat protein harbors an adenylyl cyclase catalytic center and affects responses to pathogens

Chantal Bianchet[a+], Aloysius Wong[b+], Mara Quaglia[c], May Alqurashi[d], Chris Gehring[a,d], Vardis Ntoukakis[e,f] and Stefania Pasqualini[a]*

[a] Department of Chemistry, Biology and Biotechnology, University of Perugia, Borgo XX giugno, 74, 06121 Perugia, Italy.

[b] College of Science and Technology, Wenzhou-Kean University, 88 Daxue Road, Ouhai, Wenzhou, Zhejiang Province, 325060, China.

[c] Department of Agricultural, Food and Environmental Sciences, University of Perugia, Borgo XX giugno, 74, 06121 Perugia, Italy.

[d] Biological and Environmental Sciences and Engineering Division, 4700 King Abdullah University of Science and Technology, Thuwal 23955-6900, Saudi Arabia.

[e] School of Life Sciences, University of Warwick, CV4 7AL, Coventry, UK.

[f] Warwick Integrative Synthetic Biology Centre, The University of Warwick, Coventry, CV4 7AL, Coventry, UK

*Corresponding author: stefania.pasqualini@unipg.it

[+]These authors contributed equally to this work

ABSTRACT

Adenylyl cyclases (ACs) catalyse the formation of the second messenger cAMP from ATP. Here we report the characterization of an *Arabidopsis thaliana* leucine-rich repeat (LRR) protein (*At3g14460*; AtLRRAC1) as an adenylyl cyclase. Using an AC-specific search motif supported by computational assessments of protein models we identify an AC catalytic center within the N-terminus and demonstrate that AtLRRAC1 can generate cAMP *in vitro*. Knock-out mutants of *AtLRRAC1* have compromised immune responses to the biotrophic fungus *Golovinomyces orontii* and the hemibiotrophic bacteria *Pseudomonas syringae*, but not against the necrotrophic

fungus *Botrytis cinerea*. These findings are consistent with a role of cAMP-dependent pathways in the defence against biotrophic and hemibiotrophic plant pathogens.

Keywords

cAMP; Adenylyl cyclase; *Arabidopsis thaliana; Botrytis cinerea*; *Golovinomyces orontii*; *Pseudomonas syringae* pv. *tomato*.

Abbreviations

Adenylyl cyclase, AC; adenosine 5'-triphosphate, ATP; cyclic adenosine 3′,5′-monophosphate, cAMP; cyclic nucleotide gated channels, CNGC; *Arabidopsis thaliana* leucine-rich repeat adenylyl cyclase 1, AtLRRAC1; Columbia-0, Col-0; flagellin, flg22; resistance to *Pseudomonas syringae* pv. *glycinea* 1-B, RPG1-B; FLAGELLIN-SENSING 2, *fls2*; FLG22-INDUCED RECEPTOR-LIKE KINASE 1, *FRK1;* PHOSPHATE-INDUCED 1, *PHI-1;* CAM-BINDING PROTEIN 60-LIKE G, *CBP60g*; days post-inoculation, dpi; optical density at 600 nm, OD600.

Introduction

ACs (EC 4.6.1.1) are enzymes that catalyse the conversion of ATP to cAMP. Cyclic AMP acts as a key signal transducer across all living organisms ranging from simple unicellular prokaryotes such as *Escherichia coli*, to complex multicellular organisms including animals and plants. Cyclic AMP, originally discovered in mammalian cells, mediates hormone effects (Sutherland *et al*., 1968) and regulates multiple pathways (Francis *et al*., 2011) essential for adaptation and survival (Bretschneider *et al*., 1999; Biswas *et al*., 2011).

The longstanding questions of whether cAMP exists in higher plants and if it does, what is its role as a signaling molecule, are now being resolved not least because modern high-resolution detection methods have enabled sensitive and accurate cAMP quantifications both *in vitro* and *in vivo* (Gehring and Turek, 2017). Cyclic AMP has been demonstrated to have many functions in plants including: activation of protein kinases in rice leaves (Komatsu and Hirano, 1993) and the promotion of cell division in tobacco BY-2 cells (Ehsan *et al*., 1998). Furthermore, exogenously applied cAMP to *Vicia faba*, causes stomatal opening (Curvetto *et al*., 1994) and modulates ion

transport through CNGC (Maathuis and Sanders, 1996; Lemtiri-Chlieh and Berkowitz, 2004; Zelman *et al*., 2012). More recently, cAMP has also been shown to have critical functions in plant stress responses and defence (Gottig *et al*., 2009; Thomas *et al*., 2013). cAMP, apart from being implicated in activation of phytoalexin synthesis in sweet potato (*Ipomoea batatas*) (Oguni *et al*., 1976) and in early signaling events in the apoplastic oxidative burst (Bindschedler *et al.*, 2001), cAMP was also reported at the infection site initiation in pathogen-related cytosolic Ca^{2+} signaling (Ma *et al.,* 2009). Furthermore, Jiang *et al.* (2005) reported that endogenous cAMP is involved in plant defence responses against *Verticillium* toxins in Arabidopsis. It is noteworthy that many signaling pathways induced by biotic stresses depend on CNGCs activated by cAMP (Balagué *et al.,* 2003; Lu *et al.* 2016). Perhaps not surprisingly, many Arabidopsis AC candidates belong to the nucleotide-binding site-leucine-rich repeat (NBS-LRR) family, which are involved in disease resistance and are believed to bind to pathogen-associated proteins (McHale *et al.,* 2006). However, to-date, plant ACs that harbor LRR domains have not been reported. In contrast, several cGMP-generating enzymes, guanylyl cyclases (GCs) (e.g. AtPSKR1, AtBRI1 and AtPepR1) that harbor extracellular LRR domains linked via a transmembrane region to the GC center usually embedded at a moonlighting site within a distinct kinase domain, have already been characterized (Wong *et al.*, 2018; Xu *et al.*, 2018b). Such architecture is a common feature of plant receptor proteins (e.g. AtBRI1) where association with either a modified host protein or a pathogen protein can lead to dimerization or formation of complexes with neighboring proteins. This conformational changes at the amino-terminal and LRR domains of plant NBS-LRR proteins can then bring together cytosolic domains of the respective proteins involved in the complex formation which in turn, activates enzymatic domains among other possible signaling events including phosphorylation and ubiquitylation (De Young and Innes, 2006; Wheeler *et al*., 2017). In line with the role of orchestrating biochemical reactions essential for various plant biological responses, a direct link between the LRR domain and its GC center was observed when binding of the ligand at the extracellular receptor domain elevated intracellular cGMP levels (Kwezi *et al*., 2007).

The discovery of components of cAMP-dependent signaling pathways, as well as cAMP-interacting proteins (Donaldson *et al.* 2016) and cAMP-dependent kinases (protein kinase A;

PKA) have also been reported (e.g. Assmann, 1995; Gehring, 2010) further supporting the role of cAMP in plant signaling cascades.

However, to-date only few ACs have been experimentally tested in higher plants; these include a *Zea mays* protein that participates in polarized pollen tube growth (Moutinho *et al*., 2001), a *Nicotiana benthamiana* protein with a role in tabtoxinine-β-lactam-induced cell death (Ito, 2014), a *Hippeastrum x hybridum* protein that is involved in stress signaling (Świeżawska *et al.,* 2014), an Arabidopsis pentatricopeptide repeat-containing protein, AtPPR (At1g62590) (Ruzvidzo *et al.,* 2013), an Arabidopsis clathrin assembly protein with a predicted role in actin cytoskeletal remodeling during endocytic internalization (Chatukuta *et al.*, 2018) and an Arabidopsis K^+-uptake permease (KT/HAK/KUP7; AtKUP7, At5g09400; Al-Younis *et al.*, 2015). One possible reason for this apparent elusiveness is the evolutionary divergence of plant nucleotide cyclases where only key amino acids within the catalytic centers appear to be retained. Furthermore, in plants, many proteins exist as complex molecules consisting of primary domains and secondary moonlighting sites that may include ligand binding sites and catalytic centers (Irving *et al.,* 2018). Since these functional sites constitute only a small region of a relatively large protein complex, they cannot always be detected by BLAST searches. .While key residues in canonical cyclases may be situated distantly from each other within a single protein chain or located on different protein chains but coming together to form the catalytic pocket, plant proteins harbor moonlighting sites that contain key amino acids situated in much more closer proximity (Xu *et al*., 2018a). Therefore, rationally designed motifs containing only key residues of the catalytic centers have been implemented and have since led to the discovery of a number of novel plant ACs (Wong et al., 2018).

Here we report the discovery of a functional AC catalytic center within the N–terminal of an Arabidopsis leucine-rich repeat (LRR) protein, we demonstrate its AC activity *in vitro,* and its role in responses to pathogens. Our results, link cAMP-dependent signaling to immune responses to biotrophic and hemibiotrophic pathogens.

Material and methods

Generation of a recombinant AC domain (AtLRRAC1$^{1-232}$)

cDNA was synthesized from RNA extracted from leaf of Col-0 *Arabidopsis thaliana* using the RNeasy kit (Qiagen, Crawley UK). The cDNA sequence (*AtLRRAC1, At3g14460*) was retrieved from The Arabidopsis Information Resource (TAIR) website (https://www.arabidopsis.org). A 700bp PCR product containing the predicted AC center (*At3g14460-AC*) was amplified using a pair of gene specific primers containing *attB* flanking sequence: *attB-At3g14460* Forward (5'-GGGGACAAGTTTGTACAAAAAAGCAGGCTTAATGGCGAACTCCTATTTATCAAGT-3') and *attB-At3g14460* Reverse (5'-GGGGACCACTTTGTACAAGAAAGCTGGGTA CCCAGCAGAGATCCACATTT-3'), and cloned into the Gateway-compatible pDONR221 vector (Invitrogen, Carlsbad, USA) by BP recombination reaction according to the manufacturer's instructions (Invitrogen). The *At3g14460* AC-containing fragment was recombined into pDEST17 expression vector by LR recombination reaction (Invitrogen) to create a pDEST17-*At3g14460-AC* fusion construct containing a C-terminal His tag for affinity purification. The recombinant cDNA encoding At3g14460$^{1-232}$ (AtLRRAC1$^{1-232}$) in the pDEST17-*At3g14460-AC* fusion construct was transformed into BL21 A1 *E. coli* cells (Invitrogen) for protein expression and expressed as detailed elsewhere (Meier *et al*., 2010; Raji and Gehring, 2017).

Tryptic digest and mass spectroscopy

The identity of the purified protein is also confirmed by mass spectrometry analysis. The purified protein samples were digested by trypsin and re-solubilized in 5% acetonitrile and 0.1% formic acid and ran on the Q-Trap mass spectrometry coupled with a LC system with a LC gradient of 45 min. The resulting Q-Trap data was run on the MASCOT (Matrix Science, USA) and the Scaffold software (Proteome Software, USA) using both the Arabidopsis (TAIR10 version) and *E. coli* (Swiss-Prot version 57.15) databases. The resulting peptide sequence was analyzed by BLAST to confirm the identity, purity and coverage of the protein sample.

Computational assessment of the AC catalytic center

The AtLRRAC1$^{1-232}$ model was generated using the iterative threading assembly refinement (I-TASSER) method (Zhang, 2008). The AtLRRAC1$^{1-232}$ amino acid sequence was submitted to the I-TASSER server available on-line at: http://zhanglab.ccmb.med.umich.edu/I-TASSER/ and the model with the highest quality based on their C-score was downloaded from the server. Docking

of ATP to the AC center of AtLRRAC1$^{1-232}$ was performed using AutoDock Vina (ver. 1.1.2) (Trott and Olson, 2010). The AC center of AtLRRAC1$^{1-232}$ and ATP docking pose were analyzed and all images were created UCSF Chimera (ver. 1.10.1) (Pettersen *et al*., 2004).

In vitro adenylyl cyclase enzymatic assay and detection of cAMP

AC activity of recombinant AtLRRAC1$^{1-232}$ was assessed *in vitro* by measuring cAMP generated from a reaction mixture containing 10 µg of the purified recombinant protein, 50 mM Tris-Cl; 2 mM IBMX, 5 mM $MnCl_2$ and 1 mM ATP (Kwezi *et al*., 2007; Al-Younis *et al*., 2015), by mass spectrometry. Mass spectrometry detection and quantitation of cAMP were done according to a protocol detailed elsewhere (Wheeler *et al*., 2017).

Plant materials

Seeds of *Arabidopsis thaliana* (Col-0) and two homozygous ACs knock-out T-DNA insertion mutants, *atlrrac1-1* (SALK_138613C) and *atlrrac1-2* (SALK_051867C) (Alonso *et al*., 2003), were obtained from the Arabidopsis Stock Center (NASC; http//Arabidopsis.info) and were used for pathogen phenotyping. The seeds were surface sterilized in 70% (v/v) ethanol for 1 min and 15% (v/v) sodium hypochlorite for 3 min, then rinsed three times with sterile distilled water and re-suspended in sterile distilled water. The sterilized seeds were sown in sterile soil (Patzer Einheitserde, Manna Italia, Bolzano, Italy) that had been autoclaved twice with a 1-day interval and put into individual sterilized 5 cm pots. Once the seeds were sown, they were vernalizated at 4 °C for 2 days. They were then moved to the climatic chamber, for growth under a 12 h photoperiod with a photosynthetic photon fluence rate of 350 µmol m^{-2} s^{-1}, at 20 ±2 °C, and 60% to 75% relative humidity. Water was supplied by sub-irrigation.

Seedling Liquid Culture

For growing seedlings in liquid medium Arabidopsis seeds of Col-0, *atlrrac1-1* and *fls2* receptor mutants (Zipfel *et al.,* 2004) that were used as a negative control in all assays were sterilized as above and grown in liquid Murashige and Skoog medium (MS salts, Duchefa, The Netherlands), 1% sucrose and water under the following conditions: 10 h light/14h dark at 22°C (2 seedlings/1 ml of medium in wells of 24-well-plates).

Inoculation with G. orontii and quantification of infection levels

Pure isolates of the biotrophic pathogen *Golovinomyces orontii* (Castagne) V.P. Heluta were maintained on susceptible *Cucurbita pepo* L. and *Cucurbita maxima* Duchesne plants, which were inoculated by leaf-printing and growth in a climatic chamber at 12 h photoperiod with a photosynthetic photon fluence rate of 350 µmol m^{-2} s^{-1}, 18 ±2 °C and 60% to 75% relative humidity. Fresh conidia were harvested from infected *Cucurbita* spp. plants using a paintbrush and suspended in sterilized deionized water added with 0.04% (v/v) Tween 20® (10% v/v aqueous solution, Sigma-Aldrich Inc., St. Louis, USA) to a concentration of 5 ×10^5 conidia mL^{-1}. To have a comparable number of conidia per leaf surface, the conidial suspensions were sprayed until run-off on detached rosette leaves taken from 4-week-old Col-0, *atlrrac1-1* and *atlrrac1-2* Arabidopsis plants maintained on 1.2% water-agar (Agar Bacteriological, Biolife Italiana, S.r.l., Milan, Italy) in 9-cm-diameter Petri dishes. Control leaves were sprayed only with sterile aqueous solution of Tween 20. Dishes were incubated in a climatic chamber, under the conditions optimized for *G. orontii* growth and reported above. Pathogen growth was assessed by microscopy and qRT-PCR analysis on Col-0 and mutant *atlrrac1-1* leaf samples taken at 5 dpi. Microscopic examination was performed using a light microscope (Axiophot Zeiss, Carl Zeiss, Jena, Germany) at 10× magnification, on ethanol-cleared leaf samples stained with Trypan blue, following the method reported previously (Reuber *et al*., 1998; Ederli *et al*., 2015). Four independent experiments were set up. In each experiment, six leaves per genotype were inoculated and six randomly selected areas (2.5 mm^2) per leaf were observed, for a total of 0.15 cm^2 per leaf. For each area, the number of fungal colonies, conidiophores per colony, and conidia per colony were counted. For each parameter, the means of four experiments were subjected to one-way (genotype) analysis of variance (ANOVA) and compared using Tukey's HSD test.

For qRT-PCR analysis, genomic DNA was extracted from the inoculated leaf tissue (100 mg) using GeneJET Plant Genomic DNA kits (Thermo Scientific, Waltham, USA), according to the manufacturer instructions. Genomic DNA was also extracted from *G. orontii* fresh conidia (100 mg) harvested from infected *Cucurbita* spp using Zymo Research Fungal/ Bacterial DNA kits (Zymo Research, Irvine, CA, USA), according to the manufacturer instructions. DNA quality and amount were determined with a Nanodrop spectrophotometer (Thermo Scientific). qRT-PCR was performed using a real-time PCR detection system (CFX96™; Bio-Rad, Hercules, CA,

USA), and Eva-Green® dye (Bio-Rad), with the primers listed in the Supplementary Table S1. The qPCR mixture (20 µL) comprised 5 µL total DNA (80 ng), 10 µL SsoFast EvaGreen Supermix (Bio-Rad), 0.4 µM of each primer, and sterile distilled water to the final volume. The qPCR thermal profile for *G. orontii* quantification was reported previously (Wessling and Panstruga, 2012). Three technical and three biological replicates (each with six leaves) were performed. Standard curves were designed by plotting the logarithmic values of given amounts of plant or fungal DNA (10, 20, 40, 80, 100 ng) *versus* the corresponding cycle threshold (Ct) values. Data were subject to one-way (genotype) analysis of variance (ANOVA) and compared by Tukey's HSD test.

Inoculation with Botrytis cinerea and quantification of infection levels

The isolate of the necrotrophic pathogen *B. cinerea* Pers. ex Fr. and the inoculum preparation at the concentration of 1×10^5 conidia mL^{-1} were as reported by Ederli et al. (2015). The conidial suspension was drop inoculated onto detached rosette leaves (two drops per leaf, 5 µL conidial suspension per drop). These leaves were taken from 4-week-old Col-0 and *atlrrac1-1* Arabidopsis plants maintained on 1.2% water-agar in 9-cm-diameter Petri dishes. The dishes were incubated in a climatic chamber, under the conditions reported above for plant growth. High humidity (about 95%) was maintained within each Petri dish by sealing them with cellophane. Three experiments were set up, in each experiment 24 leaves per genotype were inoculated for a total of 42 lesions observed. Necrotic lesion areas were measured at 5 dpi. The means of the three experiments were subjected to one-way (genotype) analysis of variance (ANOVA), and compared using Tukey's HSD test. Genomic DNA was extracted from *B. cinerea* mycelia (100 mg) harvested from 10-day-old colonies grown in 9-cm-diameter Petri dishes on Potato Dextrose Agar medium (Biolife Italiana S.r.l., Milan, Italy). For fungal DNA extraction, Zymo Research Fungal/ Bacterial DNA kits were used (Zymo Research, Irvine, CA, USA), according to the manufacturer instructions. For *B. cinerea* quantification, the qPCR was performed as reported for *G. orontii*.

Inoculation with Pseudomonas syringae pv. tomato DC3000 and AvrRpm1

Pseudomonas syringae pv. *tomato* DC3000 (*Pst*) and *Pst* DC3000 carrying the avirulence gene *AvrRpm1* (*Pst AvrRpm1*) were grown overnight at 28°C in King's medium containing the

appropriate antibiotics (50 mg/L rifampicin, 50 mg/L kanamycin). Bacteria were pelleted, washed three times with 10 mM $MgCl_2$, resuspended and diluted in 10 mM $MgCl_2$ to the desired concentration (10^5 colony forming units mL^{-1}, OD_{600} 0.001). The bacterial solution was inoculated on five-week-old Arabidopsis plants (Col-0, *atlrrac1-1*and *atlrrac1-2*) by syringe infiltration of leaves. Population counts were performed at zero and three dpi for DC3000 infection and only at 3 dpi for *AvrRpm1*. In both cases, serial dilutions of leaf extracts were plated on KB agar containing specific antibiotics. Each data point represents the average of 6 replicates, each containing two leaf discs from different plants. These experiments were repeated three times. Data were subject to two-way (genotype) analysis of variance (ANOVA) and compared by Tukey's HSD test.

Flagellin (flg22) treatment and analysis of transcripts of immune-related genes

Four two-week-old seedlings of Col-0 and *atlrrac1-1* grown in MS medium were transferred in liquid MS and elicited with flg22 peptide to a final concentration of 100 nM. Seedling were collected prior and after one hour of treatment, frozen in liquid nitrogen and stored at −80°C for RNA extraction. Total RNA was extracted from the frozen and homogenized leaf tissues (100 mg FW), using PureLink RNA Mini Kit (Thermo Scientific), according to the manufacturer instructions. RNA samples were treated with Turbo DNA-free DNase (Thermo scientific) and quantified with a Nanodrop spectrophotometer (Thermo scientific). cDNA synthesis was obtained with Super Script II RT (Invitrogen) and the qPCR thermal profile consisted of denaturation at 94 °C for 2 min, 40 repeated cycles of 94 °C for 15 sec 62 °C for 1 min. Melting curve was run from 55 to 95°C with 0.5 sec time interval to ensure the specificity of product. Three technical and three biological (4 seedling each) replicates were performed, using gene-specific primers reported in Table S1 (*Tubulin alpha 4* as reference gene). Data were subject to two-way (genotype) analysis of variance (ANOVA) and compared by Tukey's HSD test.

Results and Discussion

Identification of an AC catalytic center in AtLRRAC1

Since the complete Arabidopsis genome is available (The Arabidopsis Genome Initiative 2000), search motifs intended for the identification of the seemingly elusive GCs in higher plants have

been constructed based on functionally assigned residues in the catalytic centers of GCs across species. These carefully curated motifs have led to the identification of a number of candidate GCs in plants (Ludidi and Gehring 2003; Wong and Gehring, 2013), many of which have since been experimentally proven to harbor functional GC centers and affecting a growing number of biological functions *in planta* (Kwezi *et al*., 2011; Mulaudzi *et al.,* 2011; Turek and Gehring, 2016; Wheeler *et al.,* 2017). In plant GCs, the functionally tested 14-amino acid-long search motif is characterized by the residue in position 1 [R, K or S] that forms the hydrogen bond with guanine; the residue in position 3 [CTGH] that confers substrate specificity; and the residue in position 12, 13 or 14 [K or R] that stabilizes the transition state from GTP to cGMP. The amino acid [D or E] at 1-3 residues downstream from position 14 of the motif, participates in Mg^{2+}/Mn^{2+}-binding (Tucker *et al*., 1998) while situated in between the 1st and 3rd positions of the motif, is a [Y, F or W] core (Fig. 1a). In an attempt to identify candidate ACs in higher plants, we have substituted the 3rd position of the GC motif [C, G, T or H] with [D or E] (Fig. 1a) that confers specificity for the substrate ATP since the AC and GC centers in organisms across species differ only in their substrate preference (Tucker *et al*., 1998; Roelofs *et al*., 2001; Gehring, 2010; Wong and Gehring, 2013). This amino acid substitution step was performed based on the rationale used in previous studies, canonical GCs have been converted to functional ACs where they preferentially catalyse ATP over GTP and *vice versa* through site-directed mutagenesis of the residue responsible for substrate recognition (Tucker *et al*., 1998; Roelofs *et al*., 2001). We then searched the Arabidopsis proteome using this curated AC-specific motif ([**R**]X{5,20}[**RKS**][YFWP][**DE**]X{0,1}[VIL]X{5}[VIL] X[**KR**]X{1,3}[**DE**]) that also includes an [R] residue between 5 and 20 amino acids upstream of position 1 for pyrophosphate binding (Liu *et al*., 1997) and added aliphatic amino acids in position 4 or 5 and 9 or 10 respectively for greater stringency (e.g. Kwezi *et al*., 2007; Meier *et al*., 2010; Qi *et al*., 2010; Kwezi *et al*., 2011). We retrieved a total of 91 candidates harbouring this AC center and selected At3g14460 (AtLRRAC1) for further computational and experimental validations since this protein contains an additional two AC relaxed core motifs ([**RKS**]X[**DE**]X{9,11}[**KR**]X{1,3}[**DE**]), one closer to the N-terminal and the other at the C-terminal (Fig. 1b). We have also noted a NB-ARC domain (van der Biezen and Jones, 1998b) spanning from amino acid 190 to 300. Interestingly, it is the most N-terminal core motif (K121-K134) that is highly conserved at the same position in many higher plants (Fig. 1c).

Next, we adopted a computational approach to assess the feasibility of the AC center (K121-K134) of AtLRRAC1 to bind ATP and subsequently catalyse its conversion to cAMP. We have modelled an AtLRRAC$^{1-232}$ fragment that was also generated for the subsequent *in vitro* functional assay, by iterative threading. The AtLRRAC$^{1-232}$ model is consistent with the presence of a solvent exposed AC center (K121-K134) located at the base of a distinctive cavity that allows for unimpeded substrate interactions and presumably also for catalysis (Fig. 2a). We further probed this AC center by molecular docking of ATP, since favourable substrate interaction is pre-requisite for catalysis and indeed, ATP docks at this AC center with a good free energy. As for the binding pose, the negatively charged phosphate end of ATP points towards K134, while the adenosine end is orientated towards K121 and E123 (Fig. 2b and c). Since this ATP orientation is reminiscence of that in a recently characterized AC center in AtKUP7 (Al-Younis *et al*., 2015) and in structurally resolved and experimentally confirmed GC centers (Wheeler *et al*., 2017; Wong *et al*., 2015) identified using a similar motif-based approach, it appeared likely that the AC center (K121-K134) of AtLRRAC1 is capable of performing the catalytic roles (Wong and Gehring, 2013; Wong *et al.,* 2018).

In vitro AC activity of recombinant AtLRRAC1$^{1-232}$

To test if AtLRRAC1 generates cAMP *in vitro*, the fragment (AtLRRAC1$^{1-232}$) containing the predicted AC center was expressed in *E. coli* and affinity purified. The mass of this recombinant protein was predicted to be 26 kDa using the ProtParam tool provided by the ExPasy Proteomics Server (http://au.expasy.org/tool/.protpatram.html) which is consistent with the molecular weight of the protein band observed on a 10% (w/v) polyacrylamide gel of SDS-PAGE-separated protein-containing fractions (Fig. 3 b). The amino acids sequence and purity of the recombinant protein was also confirmed by mass spectrometry analysis prior to enzymatic assay (see methods detailed under "tryptic digestion and mass spectroscopy"). The AC activity of AtLRRAC1$^{1-232}$ was tested in a reaction mixture containing ATP and with either Mg^{2+} or Mn^{2+} as the cofactor. We undertook a high resolution detection method, liquid chromatography tandem mass spectrometry (LC-MS/MS), to evaluate cAMP production by the AtLRRAC1$^{1-232}$ recombinant protein and specifically identified the presence of the unique product ion at m/z 136.06 $[M+H]^+$ that is obtained via High Collision Dissociation (HCD) of the protonated cAMP precursor ion (m/z 330.06). Figure 3 c shows a representative ion chromatogram of cAMP consisting of the

parent peak and the resulting product ion peak that is used for quantitation based on a pre-calibrated cAMP standard curve (Fig. 3 a). Figure 3 c marks the molecular mass of cAMP (m/z 330.06) and its corresponding product ion peak (m/z 136.6 $[M+H]^+$). The recombinant protein generated 23.74 ± 1.05 pmol/µg protein of cAMP in the presence of Mn^{2+} (Fig. 3) but only insignificant amounts of cAMP in the presence of Mg^{2+} (Fig. S1) after 25 min of enzymatic reaction (n = 3), whereas in un-induced bacterial protein extract, cAMP was not detectable above background. This suggests that the AC activity of AtLRRAC1$^{1-232}$ has a specific preference for Mn^{2+}, as a co-factor, much like the AC activity of AtKUP7 (Al-Younis *et al*., 2015) and the GC activities of similar plant GC centers including AtBRI1-GC (Wheeler *et al*., 2017; Kwezi *et al*., 2007), AtPEPR1-GC (Qi *et al*., 2010) and AtNOGC1 (Mulaudzi *et al*., 2011). Notably, the AtLRRAC1$^{1-232}$ activity is one order of magnitude higher than AtKUP7 that generated 42.5 fmol/µg protein (Al-Younis *et al*., 2015) but is 1-5 times lower than the typical animal ACs. We also noted that plant nucleotide cyclases (ACs and GCs) have shown consistently lower activities than their animal counterpart, presumably due to a more intricate regulatory role afforded to such AC and GC centers that may enable plant cells to rapidly switch from one cyclic mononucleotide-dependent signaling network to another in localized cellular micro-environments (Muleya *et al*., 2014; Wong *et al*., 2015; Irving *et al.*, 2018; Kwezi *et al.*, 2018).

Inferring and testing biological functions of AtLLRAC1

AtLRRAC1 contains an NB-ARC and an LRR domain that are defined as signaling motifs found in bacteria and eukaryotes and are shared by classical plant resistance (*R*) gene products and regulators of cell death in animals (van der Biezen and Jones1998a; Jones *et al.*, 2016; Urbach and Ausubel, 2017). A recent bioinformatic analysis has characterised the *AtLRRAC1* as a "gatekeeper" R gene, belonging to one of the four distinct cluster of NLRs loci sharing syntenic orthologs across at least ten plant genomes (Hofberger *et al*., 2014). As reported (Ashfield *et al*., 2004; Ashfield *et al*., 2014) *AtLRRAC1* is a putative *R* gene closely related to the soybean *Rpg1-b*, that confers resistance against the pathogen *P. syringae* pv. *glycinea*. We also noted that the gene is transcriptionally up-regulated by *P. parasitica* as well as FLAG22 (see Genevestigator at http://genevestigator.ethz.ch) suggesting that *AtLRRAC1* could have a role in plant immunity.

Basal plant immunity against pathogens provides a pre-infection resistance layer, that involves recognition of conserved structural components of pathogen such as flagellin or chitin, also

referred to pathogen-associated molecular patters (PAMPs) ultimately leading to PAMP-triggered immunity (PTI) (Jones and Dangl, 2006; Bigeard and Colcombet, 2015). A second layer of the plant defence system involves intracellular receptors that are products of the resistance (R) genes. These receptors recognize the products of pathogen avirulence (*Avr*) genes, leading to rapid activation of defence responses such as the hypersensitive response (HR) at the infection sites. This layer of defence is often referred as effector-triggered immunity (ETI) (Jones and Dangl, 2006; Bigeard and Colcombet, 2015).

To test the hypothesis that *AtLRRAC1* has a role in plant immunity, we investigated the biological role of this gene in response to *Golovinomyces orontii* and *Botrytis cinerea*. *R* genes conferring resistance against the biotrophic fungus *Golovinomyces orontii* are well known (Xiao *et al*., 2001; Wang *at al.,* 2009). The two homologous *A. thaliana* R genes, *RPW8.1* and *RPW8.2,* confer resistance to the *Golovinomyces* spp. fungi, the causal agent of the powdery mildew disease (Xiao *et al*., 2001). However, specific recognition of necrotrophic pathogens by similar mechanism used by biotrophs has not been documented (Birkenbihl and Somssich, 2011). With the exception of *Arabidopsis thaliana* RESISTANCE TO LEPTOSPHAERIA MACULANS 3 (RLM3), a R-protein implicated in broad immunity to several necrotrophs, no *R*-gene has been specifically associated with resistance to necrotrophs such as *Botrytis cinerea* (Mengiste, 2012). *G. orontii* and *B. cinerea* have different lifestyles and promote different selection pressures on host plants. *G. orontii* is an obligate biotroph that feeds on living host cells using a specialized structure known as a haustorium (Micali *et al*., 2011), while *B. cinerea* is a necrotrophic plant pathogen that kills host cells at the beginning of the infection process using enzymes and toxins, and then feeds on the dead plant tissues (Jiang *et al*., 2016). In Arabidopsis, the infection processes of both pathogens require approximately 4-7 days post inoculation (dpi). Infection begins with conidium germination and after penetration and colonization, they conclude with the formation of new conidia (sporulation) that represent the inocula for subsequent infections (Jiang *et al*., 2016).

Firstly, we tested the expression level of *AtLRRAC1* encoding gene in Col-0 plants. Gene expression study indicated that *AtLRRAC1* is not constitutively expressed in uninoculated control leaves but was induced at 3 and 5 dpi at the time of *G. orontii* sporulation phase (Fig. S2). As

expected, in loss-of-function mutants (*atlrrac1-1* and *atlrrac1-2*) the gene was not expressed (Fig. S2).

To quantify the susceptibility to *G. orontii* in the Col-0 and the loss-of-function mutant lines, Trypan-blue-stained leaves were examined under the microscope (Fig. 4). Microscopic examination in the conidiation phase of the *G. orontii* life cycle allows the characterization of small mutant sets (Wessling and Panstruga, 2012). Thus, in a screening among genotypes with higher and lower susceptibilities, the number of conidiophores and/or conidia is a reliable parameter to quantify host susceptibility (Gollner *et al*., 2008). At 5 dpi, the number of colonies per leaf area on detached leaves inoculated with *G. orontii* was significantly higher on *atlrrac1-1* compared to Col-0 (+19%; P = 0.046; Fig. 4 a). Furthermore, on *atlrrac1-1*, *G. orontii* colonies produced significantly more conidiophores per colony (+77%; P = 0.0024 Fig. 4 b) and conidia per colony (+96%; P = 0.016; Fig. 4c), compared to those on Col-0. Representative images of Trypan-blue-stained leaves are shown in Fig. S3 a and b. In order to confirm that the *atlrrac1-1* phenotype seen with the disease susceptibility assay is due to the disruption of *AtLRRAC1* gene, we analysed the response against *G. orontii* of the homozygous knock-out independent T-DNA insertion line *atlrrac1-2*. *Atlrrac1-2* plants showed an increased development of this biotrophic fungus, as evaluated through the number of conidiophores (+155%; P = 0,000387) and conidia (+87%; P = 0,003384) per colony, compared to Col-0 (Fig. 4 e and f), whereas the number of colonies per leaf area was higher in *atlrrac1-2* with respect to Col-0, although the difference was not statistically significant (Fig. 4 d). The increased development of *G. orontii* infection on *atlrrac1-1* detected by microscopy, was also confirmed by quantification of the fungal biomass based on qRT-PCR analysis. At 5 dpi the *G. orontii* biomass was significantly higher on *atlrrac1-1* compared to Col-0 (+48%; P = 0.046; Fig. S3 c). Thus, the late activation of *AtLRRAC1* (Fig. S2) could play a role during the sporulation phase of *G. orontii* infection. The suppressed expression of the *AtLRRAC1* makes the mutants more susceptible to *G. orontii* than Col-0. In contrast, in leaves inoculated with the necrotrophic pathogen *B. cinerea*, there were no significant differences for either lesion diameter or fungal biomass between Col-0 and *atlrrac1-1* at 5 dpi (Fig. S4). Overall, our results are consistent with a role for the *AtLRRAC1* in defence against the biotrophic *G. orontii* but not the necrotrophic *B. cinerea.*

In order to further investigate the role of *AtLRRAC1* in plant defence against pathogens, we evaluated the phenotype of Col-0, *atlrrac1-1* and *atlrrac1-2* mutant plants inoculated with the hemibiotrophic bacterium *P. syringae* pv. *tomato* (*Pst*) DC3000 and *Pst* DC3000 carrying either an empty vector (EV) or the *AvrRpm1* effector. The results obtained from the bacterial growth assays with DC3000 showed that the knocking-out of *AtLRRAC1* gene renders the two mutants lines more susceptible than Col-0 (Fig. 5 a and b). Instead, when the three genotypes were challenged with *Pst* carrying the *AvrRpm1* effector no significant differences in the bacterial growth were found at 3 dpi (Fig. 5 c), suggesting that *AtLRRAC1* is not involved in the ETI response pathway trigged by this effector. To uncover the possible involvement of *AtLRRAC1* in PTI signalling, the expression of early induced immune-related genes was investigated in *atlrrac1-1* following elicitation with the bacterial derived pathogen-associated molecular patterns (PAMPs) flg22 (Macho *et al.,* 2014). The *fls2* receptor mutant (Zipfel *et al.,* 2004) was used as a negative control. The flg22-triggered immune-related genes *FRK1*, *PHI-1* (Macho *et al.,* 2014), and *CBP60g* (Wang *et al.,* 2011) were severely inhibited in *atlrrac1-1* (Fig. 6), and this is consistent with a role of *AtLRRAC1* in the flg22-induced PTI signaling.

What are the possible links between responses to biotrophic and hemibiotrophic pathogen and cyclic nucleotide-dependent signaling? Previously, we have reported the temporal signatures of ozone (O_3)-induced hydrogen peroxide (H_2O_2) and nitric oxide (NO) generation, their effect on cGMP generation, and the consequent transcriptional changes of genes diagnostic for stress responses in tobacco (Pasqualini *et al*., 2009). We have also shown that the early response of the phenylalanine ammonia lyase gene (*PALa*) and the late response of the gene encoding the pathogenesis-related protein (*PR1a*) show critical dependence on cGMP and importantly, that differential cGMP signatures occur in responses to virulent and avirulent *Pst* strains (Meier *et al*., 2009). Accordingly, a key role of cGMP in the induction of systemic acquired response in plants challenged with avirulent pathogens has been reported (Hussain *et al.,* 2016). These observations were an indication that the growing family of structurally diverse molecules with functional mononucleotide cyclase domains (ACs and GCs), have critical and specific roles in many plant processes including defence against pathogens (Meier *et al*., 2007). It has also been reported that the levels of cAMP increased in response to biotic stress (Ma *et al*., 2009) and that cAMP influences cytosolic Ca^{2+} concentration by modulating CNGCs activity (Talke *et al*., 2003; Ali *et al*., 2007) as well as other downstream targets such as cAMP-dependent kinases and

phosphorylation. Furthermore, cAMP-dependent changes of the Arabidopsis proteome implicated cAMP in abiotic and biotic stress responses as well as direct or indirect effects on energy metabolism (Alqurashi *et al*., 2016).

In conclusion, the results of this study show that the putative R protein AtLRRAC1 containing LRR-NB-ARC domain can generate cAMP *in vitro*. In addition, knock-out mutants have compromised defence against biotrophic and hemibiotrophic pathogens, while the response to necrotrophs do not appear affected. A possible function of *AtLRRAC1* as a classical *R*-gene recognizing effectors from *G. orontii* and *Pst* DC3000 cannot be excluded but the data presented points towards a role of AC activity in plant immunity.

Together, these results suggest that *AtLRRAC1* is part of a complex response system to biotrophic and hemibiotrophic pathogens that signals through cAMP to mediate both short- and long-term adaptive responses to biotic stress.

References

Ali, R., Ma W., Lemtiri-Chlieh, F., Tsaltas, D., Leng, Q., von Bodman, S., Berkowitz, G.A., 2007. Death don't have no mercy and neither does calcium: *Arabidopsis* CYCLIC NUCLEOTIDE GATED CHANNEL2 and innate immunity. Plant Cell 19, 1081-1095.

Alonso, J., Stepanova, A.N., Leisse, T.J., Kim, C.J., Chen, H., Shinn, P., Stevenson, D.K., Zimmerman, J., Barajas, P., Cheuk, R., Gadrinab, C., Heller, C., Jeske, A., Koesema, E., Meyers, C.C., Parker, H., Prednis, L., Ansari, Y., Choy, N., Deen, H., Geralt, M., Hazari, N., Hom, E., Karnes, M., Mulholland, C., Ndubaku, R., Schmidt, I., Guzman, P., Aguilar-Henonin, L., Schmid, M., Weigel, D., Carter, D.E., Marchand, T., Risseeuw, E., Brogden, D., Zeko, A., Crosby, W.L., Berry, C.C., Ecker, J.R., 2003. Genome-wide insertional mutagenesis of *Arabidopsis thaliana*. Science 301, 653-657.

Alqurashi, M., Gehring, C., Marondedze, C., 2016. Changes in the *Arabidopsis thaliana* proteome implicate cAMP in biotic and abiotic stress responses and changes in energy metabolism. Int. J. Mol. Sci. doi:10.3390/ijms17060852.

Al-Younis, I., Wong, A., Gehring, C., 2015. The *Arabidopsis thaliana* K^+-uptake permease 7 (AtKUP7) contains a functional cytosolic adenylate cyclase catalytic center. FEBS Lett. 589, 3848-3852.

Ashfield, T., Ong, L.E., Nobuta, K., Schneider, C.M., Innes, R.W., 2004. Convergent evolution of disease resistance gene specificity in two flowering plant families. Plant Cell 16, 309-318.

Ashfield, T., Redditt, T., Russell, A., Kessens, R., Rodibaugh, N., Galloway, L., Kang, Q., Podicheti, R., Innes, R.W., 2014. Evolutionary relationship of disease resistance genes in soybean and Arabidopsis specific for the *Pseudomonas syringae* effectors AvrB and AvrRpm1. Plant Physiol. 166, 235-251.

Assmann, S. M., 1995. Cyclic AMP as a second messenger in higher plants (status and future prospects). Plant Physiol. 108, 885-889.

Balagué, C., Lin, B., Alcon, C., Flottes, G., Malmström, S., Köhler, C., Neuhaus, G., Pelletier, G., Gaymard, F., Roby, D., 2003. HLM1, an essential signaling component in the hypersensitive response, is a member of the cyclic nucleotide–gated channel ion channel family. Plant Cell, 15, 365-379.

Bigeard J., Colcombet, J., Hirt, H. 2015. Signaling Mechanisms in Pattern-Triggered Immunity (PTI). Mol. Plant 8, 521–539.

Bindschedler, L.V., Minibayeva, F., Gardber, S.L., Gerrish, C., Davies, D.R., Bolwell, G.P., 2001. Early signalling events in the apoplastic oxidative burst in suspension cultured French bean cells involve cAMP and Ca^{2+}. New Phytol. 151, 185–194.

Birkenbihl, R. P., & Somssich, I. E., 2011. Transcriptional plant responses critical for resistance towards necrotrophic pathogens. Front. Plant Sci. 2, 76. doi.org/10.3389/fpls.2011.00076.

Biswas, A., Bhattacharya, A., Das, P.K., 2011. Role of cAMP signaling in the survival and infectivity of the protozoan parasite, *Leishmania donovani*. Mol. Biol. Int. doi:10.4061/2011/782971.

Bretschneider, T., Vasiev, B., Weijer, C.J., 1999. A model for *Dictyostelium* slug movement. J. Theor. Biol. 199, 125-136.

Chatukuta, P., Dikobe, T.B., Kawadza, D.T., Sehlabane, K.S., Takundwa, M.M., Wong, A., Gehring, C., Ruzvidzo, O., 2018. An Arabidopsis clathrin assembly protein with a predicted role in plant defense can function as an adenylate cyclase. Biomolecules doi.org/10.3390/biom8020015.

Curvetto, N., Darjania, L., Delmastro, S., 1994. Effect of two cAMP analogs on stomatal opening in *Vicia faba.* Possible relationship with cytosolic calcium concentration. Plant Physiol. Biochem. 32, 365-372.

DeYoung, B. J., & Innes, R. W. (2006). Plant NBS-LRR proteins in pathogen sensing and host defense. Nat. Immunol. 7, 1243-1249.

Donaldson, L., Meier, S., Gehring, C., 2016. The Arabidopsis cyclic nucleotide interactome. Cell Commun. Signal. doi:10.1186/s12964-016-0133-2.

Ederli, L., Dawe, A., Pasqualini, S., Quaglia, M., Xiong, L., Gehring, C., 2015. *Arabidopsis* flower specific defense gene expression patterns affect resistance to pathogens. Front. Plant Sci. doi:10.3389/fpls.2015.00079.

Ehsan, H., Reichheld, J.P., Roef, L., Witters, E., Lardon, F., Van Bockstaele, D., Van Montagu, M., Inzé, D., Van Onckelen, H., 1998. Effect of indomethacin on cell cycle dependent cyclic AMP fluxes in tobacco BY-2 cells. FEBS Lett. 422, 165-169.

Francis, S.H., Blount, M.A., Corbin, J.D., 2011. Mammalian cyclic nucleotide phosphodiesterases: molecular mechanisms and physiological functions. Physiol. Rev. 91, 651-690.

Gehring, C. and Turek, I.S., 2017. Cyclic nucleotide monophosphates and their cyclases in plant signaling. Front. Plant Sci. doi:10.3389/fpls.2017.01704.

Gehring, C., 2010. Adenyl cyclases and cAMP in plant signaling - past and present. Cell Commun. Signal. doi.org/10.1186/1478-811X-8-15.

Gollner, K., Schweizer, P., Bai, Y., Panstruga, R., 2008. Natural genetic resources of *Arabidopsis thaliana* reveal a high prevalence and unexpected phenotypic plasticity of RPW8-mediated powdery mildew resistance. New Phytol. 177, 725-742.

Gottig, N., Garavaglia, B.S., Daurelio, L.D., Valentine, A., Gehring, C., Orellano, E.G., Ottado, J., 2009. Modulating host homeostasis as a strategy in the plant-pathogen arms race. Commun. Integr. Biol. 2, 89-90.

Hofberger, J.A, Zhou, B., Tang, H., Jones, J.D.G., Schranz, M.E., 2014. A novel approach for multi-domain and multi-gene family identification provides insights into evolutionary dynamics of disease resistance genes in core eudicot plants. BMC Genomics doi.org/10.1186/1471-2164-15-966.

Hussain, J., Chen, J., Locato, V., Sabetta, W., Behera, S., Cimini, S., Griggio, F., Martinez-Jaime, S., Graf, A., Bouneb, M., Pachaiappan, R., Fincato, P., Bianco, E., Costa, A., De Gara, L., Bellin, D., De Pinto, M.C., Vandelle, E., 2016. Constitutive cyclic GMP accumulation in *Arabidopsis thaliana* compromises systemic acquired resistance induced by an avirulent pathogen by modulating local signals. Sci. Rep. doi: 10.1038/srep36423.

Irving, H.R., Cahill, D.M., Gehring, C., 2018. Moonlighting proteins and their role in the control of signaling microenvironments, as exemplified by cGMP and phytosulfokine receptor 1 (PSKR1). Front. Plant Sci. doi: 10.3389/fpls.2018.00415.

Ito, M., Takahashi, H., Sawasaki, T., Ohnishi, K., Hikichi, Y., Kiba, A., 2014. Novel type of adenylyl cyclase participates in tabtoxinine-β-lactam-induced cell death and occurrence of wildfire disease in *Nicotiana benthamiana*. Plant Signal Behav. doi:10.4161/psb.27420.

Jiang, J., Fan, L.W., Wu, W.H., 2005. Evidences for involvement of endogenous cAMP in Arabidopsis defense responses to Verticillium toxins. Cell Res. 15, 585–592.

Jiang, Z., Dong, X., Zhang, Z., 2016. Network-based comparative analysis of *Arabidopsis* immune responses to *Golovinomyces orontii* and *Botrytis cinerea* infections. Sci. Rep. doi:10.1038/srep19149.

Jones, J.D., Dangl, J.L., 2006. The plant immune system. Nature 444, 323–329.

Jones, J.D., Vance, R.E., Dangl, J.L., 2016. Intracellular innate immune surveillance devices in plants and animals. Science doi: 10.1126/science.aaf6395

Komatsu, S. and Hirano, H., 1993. Protein-kinase activity and protein-phosphorylation in rice (*Oryza sativa L.*) leaf. Plant Sci. 94, 127-137.

Kwezi, L., Meier, S., Mungur, L., Ruzvidzo, O., Irving, H., Gehring, C., 2007. The *Arabidopsis thaliana* brassinosteroid receptor (AtBRI1) contains a domain that functions as a guanylyl cyclase *in vitro*. PloS One doi.org/10.1371/journal.pone.0000449.

Kwezi, L., Ruzvidzo, O., Wheeler, J.I., Govender, K., Iacuone, S., Thompson, P.E., Gehring, C., Irving, H.R., 2011. The phytosulfokine (PSK) receptor is capable of guanylate cyclase activity and enabling cyclic GMP-dependent signaling in plants. J. Biol. Chem. 286, 22580-22588.

Kwezi, L., Wheeler, J.I., Marondedze, C., Gehring, C. and Irving, H.R., 2018. Intramolecular crosstalk between catalytic activities of receptor kinases. Plant Sig. Behav. doi.org/10.1080/15592324.2018.1430544.

Lemtiri-Chlieh, F. and Berkowitz, G. A., 2004. Cyclic adenosine monophosphate regulates calcium channels in the plasma membrane of *Arabidopsis* leaf guard and mesophyll cells. J. Biol. Chem. 279, 35306-35312.

Liu, Y., Ruoho, A.E., Rao, V.D., Hurley, J.H., 1997. Catalytic mechanism of the adenylyl and guanylyl cyclases: modeling and mutational analysis. Proc. Natl. Acad. Sci. USA 94, 13414-13419.

Lu, M., Zhang, Y., Tang, S., Pan, J., Yu, Y., Han, J., Li, Y., Du, X., Nan, Z., Sun, Q., 2016. AtCNG2 is involved in jasmonic acid-induced calcium mobilization. J. Exp. Bot. 67, 809-819.

Ludidi, N. and Gehring, C., 2003. Identification of a novel protein with guanylyl cyclase activity in *Arabidopsis thaliana*. J. Biol. Chem. 278, 6490-6494.

Ma, W., Qi, Z., Smigel, A., Walker, R.K., Verma, R., Berkowitz, G.A., 2009. Ca^{2+}, cAMP, and transduction of non-self perception during plant immune responses. Proc. Natl. Acad. Sci. USA 106, 20995-21000.

Maathuis, F. J. M. and Sanders, D., 1996. Mechanisms of potassium absorption by higher plant roots. Physiol. Plant 96, 158-168.

Macho, A.P., Schwessinger, B., Ntoukakis, V., Brutus, A., Segonzac, C., Roy, S., Kadota, Y., Oh, M.H., Sklenar, J., Derbyshire, P., Lozano-Durán, R., Malinovsky, F.G., Monaghan, J., Menke, F.L., Huber, S.C., He, S.Y., Zipfel, C., 2014. A bacterial tyrosine phosphatase inhibits plant pattern recognition receptor activation. Science 343, 1509-1512.

McHale, L., Tan, X., Koehl, P., and Michelmore, R.W., 2006. Plant NBS-LRR proteins: adaptable guards. Genome Biol. 7 212. doi: 10.1186/gb-2006-7-4-212.

Meier, S., Madeo, L., Ederli, L., Donaldson, L., Pasqualini, S., Gehring, C., 2009. Deciphering cGMP signatures and cGMP-dependent pathways in plant defence. Plant Signal Behav. 4, 307-309.

Meier, S., Ruzvidzo, O., Morse, M., Donaldson, L., Kwezi, L., Gehring, C., 2010. The Arabidopsis *wall associated kinase-like 10* gene encodes a functional guanylyl cyclase and is co-expressed with pathogen defense related genes. PLoS One doi.org/10.1371/journal.pone.0008904.

Meier, S., Seoighe, C., Kwezi, L., Irving, H., Gehring, C., 2007. Plant nucleotide cyclases: an increasingly complex and growing family. Plant Signal Behav. 2, 536-539.

Mengiste, T., 2012. Plant immunity to necrotrophs. Annu. Rev. Phytopathol., 50:267–294. doi: 10.1146/annurev-phyto-081211-172955.

Micali, C. O., Neumann, U., Grunewald, D., Panstruga, R., O'Connell, R., 2011. Biogenesis of a specialized plant-fungal interface during host cell internalization of *Golovinomyces orontii* haustoria. Cell Microbiol. 13, 210-226.

Moutinho, A., Hussey, P.J., Trewavas, A.J., Malhó, R., 2001. cAMP acts as a second messenger in pollen tube growth and reorientation. Proc. Natl. Acad. Sci. USA 98, 10481-10486.

Mulaudzi, T., Ludidi, N., Ruzvidzo, O., Morse, M., Hendricks, N., Iwuoha, E., Gehring, C., 2011. Identification of a novel *Arabidopsis thaliana* nitric oxide-binding molecule with guanylate cyclase activity *in vitro*. FEBS Lett. 585, 2693-2697.

Muleya, V., Wheeler, J.I., Ruzvidzo, O., Freihat, L., Manallack, D.T., Gehring, C., Irving H.R., 2014. Calcium is the switch in the moonlighting dual function of the ligand-activated receptor kinase phytosulfokine receptor 1. Cell Commun. Signal doi.org/10.1186/s12964-014-0060-z.

Oguni, I., Suzuki, K., Uritani I., 1976. Terpenoid induction in sweet potato roots by cyclic-3', 5'-adenosine monophosphate. Agricult. Biol. Chem. 40, 1251-1252.

Pasqualini, S., Meier, S., Gehring, C., Madeo, L., Fornaciari, M., Romano, B., Ederli, L., 2009. Ozone and nitric oxide induce cGMP-dependent and -independent transcription of defence genes in tobacco. New Phytol. 181, 860-870.

Pettersen, E. F., Goddard, T.D., Huang, C.C., Couch, G.S., Greenblatt, D.M., Meng, E.C., Ferrin, T.E., 2004. UCSF chimera - A visualization system for exploratory research and analysis. J. Comput. Chem. 25, 1605-1612.

Qi, Z., Verma, R., Gehring, C., Yamaguchi, Y., Zhao, Y., Ryan, C.A., Berkowitz, G.A., 2010. Ca^{2+} signaling by plant *Arabidopsis thaliana* Pep peptides depends on AtPepR1, a receptor with guanylyl cyclase activity, and cGMP-activated Ca^{2+} channels. Proc. Natl. Acad. Sci. USA 107, 21193-21198.

Raji, M. and Gehring, C., 2017. In vitro assessment of guanylyl cyclase activity of plant receptor kinases. Meth. Mol. Biol. 1621, 131-140.

Reuber, T. L., Plotnikova, J.M., Dewdney, J., Rogers, E.E., Wood, W., Ausubel, F.M., 1998. Correlation of defense gene induction defects with powdery mildew susceptibility in *Arabidopsis* enhanced disease susceptibility mutants. Plant J. 16, 473-485.

Roelofs, J., Meima, M., Schaap, P., Van Haastert, P.J., 2001. The *Dictyostelium* homologue of mammalian soluble adenylyl cyclase encodes a guanylyl cyclase. EMBO J. 20, 4341-4348.

Ruzvidzo, O., Dikobe, B.T., Kawadza, D.T., Mabadahanye, G.H., Chatukuta, P., Kwezi, L., 2013. Recombinant expression and functional testing of candidate adenylate cyclase domains. In: Gehring C. (eds) Cyclic Nucleotide Signaling in Plants. Methods Mol. Biol. doi:10.1007/978-1-62703-441-8_2

Sutherland, E.W., Robison, G.A., Butcher, R.W., 1968. Some aspects of biological role of adenosine 3',5'-monophosphate (Cyclic AMP). Circulation 37, 279-306.

Świeżawska, B., Jaworski, K., Pawełek, A., Grzegorzewska, W., Szewczuk, P., Szmidt-Jaworska, A., 2014. Molecular cloning and characterization of a novel adenylyl cyclase gene, *HpAC1*, involved in stress signaling in *Hippeastrum x hybridum*. Plant Physiol. Biochem. 80, 41-52.

Talke, I.N., Blaudez, D., Maathuis, F.J., Sanders, D., 2003. CNGCs: prime targets of plant cyclic nucleotide signalling? Trends Plant Sci 8, 286-293.

The Arabidopsis Genome Initiative. 2000. Analysis of the genome sequence of the flowering plant *Arabidopsis thaliana*. Nature 408, 796-815.

Thomas, L., Marondedze, C., Ederli, L., Pasqualini, S., Gehring, C., 2013. Proteomic signatures implicate cAMP in light and temperature responses in *Arabidopsis thaliana*. J. Proteom. 83, 47-59.

Trott, O. and Olson, A. J., 2010. AutoDock Vina: improving the speed and accuracy of docking with a new scoring function, efficient optimization, and multithreading. J. Comput. Chem. 31, 455-461.

Tucker, C.L., Hurley, J.H., Miller, T.R., Hurley, J.B., 1998. Two amino acid substitutions convert a guanylyl cyclase, RetGC-1, into an adenylyl cyclase. Proc. Natl. Acad. Sci. USA 95, 5993-5997.

Turek, I. and Gehring, C., 2016. The Plant Natriuretic Peptide receptor is a guanylyl cyclase and enables cGMP-dependent signaling. Plant Mol. Biol. 91, 275-286.

Urbach, J.M. and Ausubel, F.M., 2017. The NBS-LRR architectures of plant R-proteins and metazoan NLRs evolved in independent events. Proc. Natl. Acad. Sci. USA 114, 1063-1068.

van der Biezen, E. A. and Jones, J. D., 1998a. Plant disease-resistance proteins and the gene-for-gene concept. Trends Biochem. Sci. 23, 454-456.

van der Biezen, E. A. and Jones, J. D., 1998b. The NB-ARC domain: a novel signalling motif shared by plant resistance gene products and regulators of cell death in animals. Curr. Biol. 8, R226-R228.

Wang, L., Tsuda, K., Truman, W., Sato, M.., Nguyen, L.V., Katagiri, F., Glazebrook, J., 2011. CBP60g and SARD1 play partially redundant critical roles in salicylic acid signaling. Plant J. 67, 1029-1041.

Wang, W., Wen, Y., Berkey, R. and Xiao, S., 2009. Specific targeting of the Arabidopsis resistance protein RPW8.2 to the interfacial membrane encasing the fungal haustorium renders broad-spectrum resistance to powdery mildew. Plant Cell, 21, 2898–2913.

Wessling, R. and Panstruga, R., 2012. Rapid quantification of plant-powdery mildew interactions by qPCR and conidiospore counts. Plant Meth. doi.org/10.1186/1746-4811-8-35.

Wheeler, J.I., Wong, A., Marondedze, C., Groen, A.J., Kwezi, L., Freihat, L., Vyas, J., Raji, M.A., Irving, H.R., Gehring, C., 2017. The brassinosteroid receptor BRI1 can generate cGMP enabling cGMP-dependent downstream signaling. Plant J. 91, 590–600.

Wong, A. and Gehring, C., 2013. The *Arabidopsis thaliana* proteome harbors undiscovered multi-domain molecules with functional guanylyl cyclase catalytic centers. Cell Commun. Signal. doi.org/10.1186/1478-811X-11-48.

Wong, A., Gehring, C., Irving H.R., 2015. Conserved functional motifs and homology modeling to predict hidden moonlighting functional sites. Front. Bioeng. Biotechnol. doi:10.3389/fbioe.2015.00082.

Wong, A., Tian, X., Gehring, C., Marondedze, C., 2018. Discovery of novel functional centers with rationally designed amino acid motifs. Comput. Struct. Biotech. J. 16, 70-76.

Xiao, S. Y., S. Ellwood, O. Calis, E. Patrick, T. X. Li, M. Coleman, and J. G. Turner. 2001. Broad-spectrum mildew resistance in *Arabidopsis thaliana* mediated by RPW8. Science 291, 118-120.

Xu, N., Fu, D., Li, S., Wang, Y., Wong, A., 2018a. GCPred: a web tool for guanylyl cyclase functional centre prediction from amino acid sequence. Bioinformatics 34(12), 2134-2135. doi:10.1093/bioinformatics/bty067.

Xu, N., Zhang, C., Lim, L. L., Wong, A., 2018b. Bioinformatic analysis of nucleotide cyclase functional centers and development of ACPred webserver. In: Proceedings of the ACM-

BCB'18: 9th ACM International Conference on Bioinformatics, Computational Biology, and Health Informatics. August 29-September 1, 2018, Washington DC, USA. doi:10.1145/3233547.3233549.

Zelman, A.K., Dawe, A., Gehring, C., Berkowitz, G.A., 2012. Evolutionary and structural perspectives of plant cyclic nucleotide-gated cation channels. Front. Plant Sci. doi:10.3389/fpls.2012.00095.

Zhang, Y., 2008. I-TASSER server for protein 3D structure prediction. BMC Bioinformatics doi:10.1186/1471-2105-9-40.

Zipfel, C., Robatzek, S., Navarro, L., Oakeley, E. J., Jones, J. D. G., Felix, G., Boller, T., 2004. Bacterial disease resistance in Arabidopsis through flagellin perception. Nature, 428, 764–767.

Acknowledgements

This project was funded by King Abdullah University of Science and Technology, Royal Society, Biotechnology and Biological Science Research Council grants (BB/L019345/1 and BB/M017982/1) and "Fondo di Ateneo per la Ricerca di Base 2015" financed by University of Perugia. We are grateful to Aleš Lebeda and Božena Sedláková (Palacký University, Olomouc) for providing the *Golovinomyces orontii* isolates.

Additional Information

Supplementary information accompanies this paper at

Table S1- Oligonucleotide primer sequences and amplicon size (bp) used for DNA (fungal and plant) quantification and gene expression analysis by semi-quantitative and quantitative PCR.

Figure S1 - Detection of cAMP in reaction mixtures containing different cofactors by liquid chromatography tandem mass spectrometry (LC-MS/MS).

Figure S2- Quantification of *AtLRRAC1* transcripts in Arabidopsis Col-0 and mutant lines (*atlrrac1-1* and *atlrrac1*-2) inoculated with *G. orontii*.

Figure S3 - Quantification of infection levels on *atlrrac1-1* plants inoculated with *G. orontii*.

Figure S4. Pathogen growth quantification in *B. cinerea* inoculated Arabidopsis Col-0 and *atlrrac1-1* plants.

Figure legends:

Figure 1 - Structural features of AtLRRAC1 and the AC centers.

(a) The 14 amino acid core search motif of annotated and experimentally tested GCs and ACs catalytic centers. [D or E] (blue) are the residues that confer substrate specificity and [D or E] (green) bind Mg^{2+} or Mn^{2+}. (b) Amino acid sequence of AtLRRAC1 (At3g14460) with the AC motifs in bold and/or colour. The NB-ARC domain is marked in purple. (c) Alignment of the catalytic center of orthologs of At3g14460 in other plant species (top) and alignment of catalytic centers of experimentally confirmed LLR receptor kinases with guanylyl cyclase activity.

Figure 2 - Computational assessment of AtLRRAC1 AC center.

(a) Docking of ATP at the AC center of AtLRRAC1 and the interaction of ATP with the key residues at the catalytic center is shown as (b) surface and (c) ribbon models respectively. The $AtLRRAC1^{1-232}$ model shows that the AC center (magenta) is solvent-exposed. The amino acid residues implicated in interaction with ATP are coloured according to their charges in the surface models and shown as individual atoms in the ribbon model. $AtLRRAC1^{1-232}$ was modeled using the iterative threading assembly refinement (I-TASSER) method on the on-line server: http://zhanglab.ccmb.med.umich.edu/I-TASSER/ (Zhang, 2008) and ATP docking simulation was performed using AutoDock Vina (ver. 1.1.2) (Trott and Olson, 2010).

Figure 3 - Detection of cAMP by liquid chromatography tandem mass spectrometry (LC-MS/MS).

cAMP was generated from a reaction mixture containing 10 µg of the purified recombinant protein, 50 mM Tris-Cl; 2 mM IBMX, 5 mM $MnCl_2$ and 1 mM ATP. The HPLC elution profile of cAMP and a calibration curve are shown as (a) and a 10% SDS-PAGE gel of the affinity purified $At3g14460^{1-232}$ recombinant protein is shown as (b). The amount of cAMP after 25 min of enzymatic reaction was determined to be 23.74 ±1.05 pmol/µg protein (n = 3). Representative ion chromatogram of cAMP showing the parent and daughter ion peaks and their corresponding chemical structures are shown as (c).

Figure 4 - *Golovinomyces orontii* infection in Arabidopsis Col-0, *atlrrac1-1* and *atlrrac1-2* plants.

Quantification of fungal colonies per leaf area (a, d), conidiophores per colony (b, e), and conidia per colony (c, e) in Col-0, *atlrrac1-1* and *atlrrac1-2* plants inoculated with *G. orontii* at 5 dpi. Data are means ±SE of four independent experiments and were subjected to one-way (genotype) analysis of variance (ANOVA) and compared by Tukey's HSD test. In each experiment, six leaves per genotype were inoculated and six randomly selected areas (2.5 mm^2) per leaf were assessed (total 0.15 cm^2 per leaf).

Figure 5 - ***Plant defence responses after Pseudomonas syringae pv. tomato DC3000 and DC3000 (AvrRpm1) inoculation in Arabidopsis Col-0, atlrrac1-1 and atlrrac1-2 plants.***
Bacterial growth was detected in leaves of five-week-old Col-0, *atlrrac1-1* and *atlrrac1-2* plants syringe-infiltrated with *Pst* DC3000, DC3000 empty vector and DC3000 *AvrRpm1*. Bacterial growth was detected immediately after (0 dpi) *Pst* DC3000 infiltration and after 3 dpi in Col-0 and *atlrrac1-1* (a) and Col-0 and *atlrrac1-2* (b); (c): bacterial growth was detected after 3 dpi in Col-0, *atlrrac1-1* and *atlrrac1-2* infiltrated with Pst DC3000 *AvrRpm1* and DC3000 empty vector (EV). Values are means ±SE, that were subject to two-way analysis of variance (ANOVA) and compared by Tukey's HSD test. Different letters indicate significant differences ($p \leq 0.05$).

Figure 6 - ***Plant defence responses after flg22 treatment in Arabidopsis Col-0 and atlrrac1-1 plants.***
Quantitative reverse transcription–polymerase chain reaction analyses of PAMP-induced (100 nM flg22) genes *FRK1*(a), *PHI1* (b) and *CBP60g* (c) prior (-flg22) and one hour after flg22-induction (+flg22). Data are means ±SE, that were subject to two-way analysis of variance (ANOVA) and compared by Tukey's HSD tests. Different letters indicate significant differences ($p \leq 0.01$).

a AC Core motif:

[RKS]X[DE]X{9,11}[KR]X{1,3}[DE]

b

1 60

MANSYLSSCANVMVERINTSQELVELCKGKSSSALLKRLKVALVTANPVLADADQRAEHV
REVKHWLTGIKDAFFQAEDILDELQTEALRRRVVAEAGGLGGLFQNLMAG**R**EAIQKKIEP
KM**E**K**V**V**R**L**L**E**H**H**V**K**H**I**E**V**IGLKEYSET**R**EPQW**R**QASR**SRPDDLPQGRLVGRVED**KLALVN
LLLSDDEISI**GKPAVISVVGMPGVGKTTLTEIVFNDYRVTEHFEVKMWISAGINFNVFTV
TKAVLQDITSSAVNTEDLPSLQIQLKKTLSGKRFLLVLDDFWSESDSEWESFQVAFTDAE
EGSKIVLTTRSEIVSTVAKAEKIYQMKLMTNEECWELISRFAFGNISVGSINQELEGIGK
RIAEQCKGLPLAARAIASHLRSKPNPDDWYAVSKNFSSYTNSILPVLKLSYDSLPPQLKR
CFALCSIFPKGHVFDREELVLLWMAIDLLYQPRSSRRLEDIGNDYLGDLVAQSFFQRLDI
TMTSFVMHDLMNDLAKAVSGDFCFRLEDDNIPEIPSTTRHFSFSRSQCDASVAFRSICGA
EFLRTILPFNSPTSLESLQLTEKVLNPLLNALSGLRILSLSHYQITNLPKSLKGLKLLRY
LDLSSTKIKELPEFVCTLCNLQTLLLSNCRDLTSLPKSIAELINLRLLDLVGTPLVEMPP
GIKKLRSLQKLSNFVIGRLSGAGLHELKELSHLRGTLRISELQNVAFASEAKDAGLKRKP
FLDGLILKWTVKGSGFVPGSFNALACDQKEVLRMLEPHPHLKTFCIESYQGGAFPKWLGD
SSFFGITSVTLSSCNLCISLPPVGQLPSLKYLSIEKFNILQKVGLDFFFGENNSRGVPFQ
SLQILKFYGMPRWDEWICPELEDGIFPCLQKLIIQRCPSLRKKFPEGLPSSTEVTISDCP
LRAVSGGENSFRRSLTNIPESPASIPSMSRRELSSPTGNPKSDASTSAQPGFASSSQSND
DNEVTSTSSLSSLPKDRQTEDFDQYETQLGSLPQQFEEPAVISARYSGYISDIPSTLSPY
MSRTSLVPDPKNEGSILPGSSSYQYHQYGIKSSVPSPRSSEAIKPSQYDDDETDMEYLKV
TDISHLMELPQNLQSLHIDSCDGLTSLPENLTESYPNLHELLIIACHSLESFPGSHPPTT
LKTLYIRDCKKLNFTESLQPTRSYSQLEYLFIGSSCSNLVNFPLSLFPKLRSLSIRDCES
FKTFSIHAGLGDDRIALESLEIRDCPNLETFPQGGLPTPKLSSMLLSNCKKLQALPEKLF
GLTSLLSLFIIKCPEIETIPGGGFPSNL**R**TLCISLCDKLTP**RIEWGLRDLENLRNLE**IDG
GNEDIESFPEEGLLPKSVFSLRISRFENLKTLNRKGFHDTKAIETMEISGCDKLQISIDE
DLPPLSCLRISSCSLLTETFAEVETEFFKVLNIPYVEIDGEIFS(1424)

c

At3g14460	**..KMEKVVRLLEHHV-KHI-E..**
Brassica napus	**..KMENVVRLLEHHV-RHI-E..**
Camelina sativa	**..KMEKVVRLLEHHV-KHI-E..**
Tarenaya hassleriana	**..RMEEIVDQLEQLV-RSLQE..**
Vitis vinifera	**..RVEEIIDRLEDMA-RDR-D..**
Prunus persica	**..KIEEIIERLDFIE-KKK-D..**
Experimentally confirmed LRR receptor kinases:	
AtPSKR1	**..SFGVVLLELLTDK-RPV-D..**
AtBRI1	**..SYGVVLLELLTGK-RPT-D..**
AtPep-R1	**..SYGVVLLELVTRK-RAV-D**
AtPNP-R1	**..KLTFVRTLETLDLSRNLIF..**

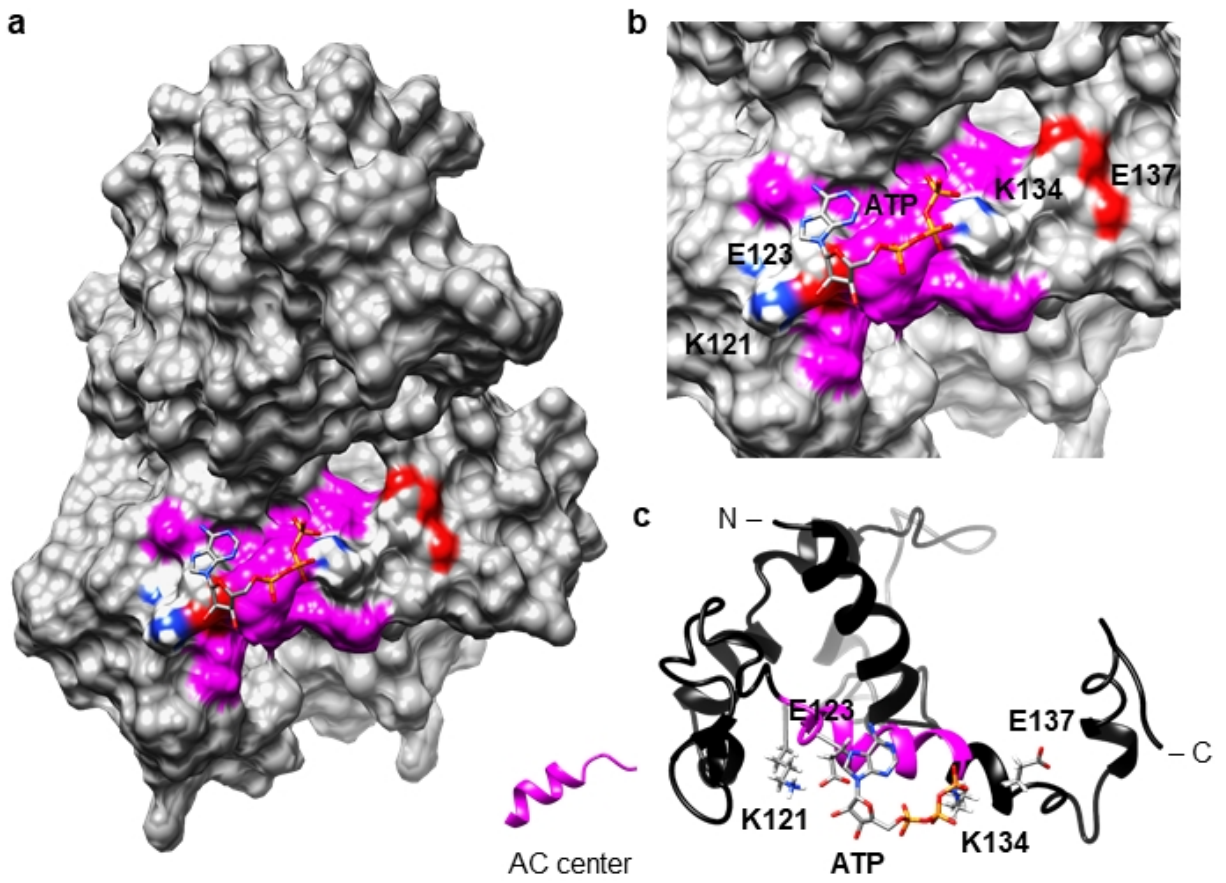
a
b
ATP
K134
E137
E123
K121
c
N –
E123
E137
– C
K121
K134
ATP
AC center

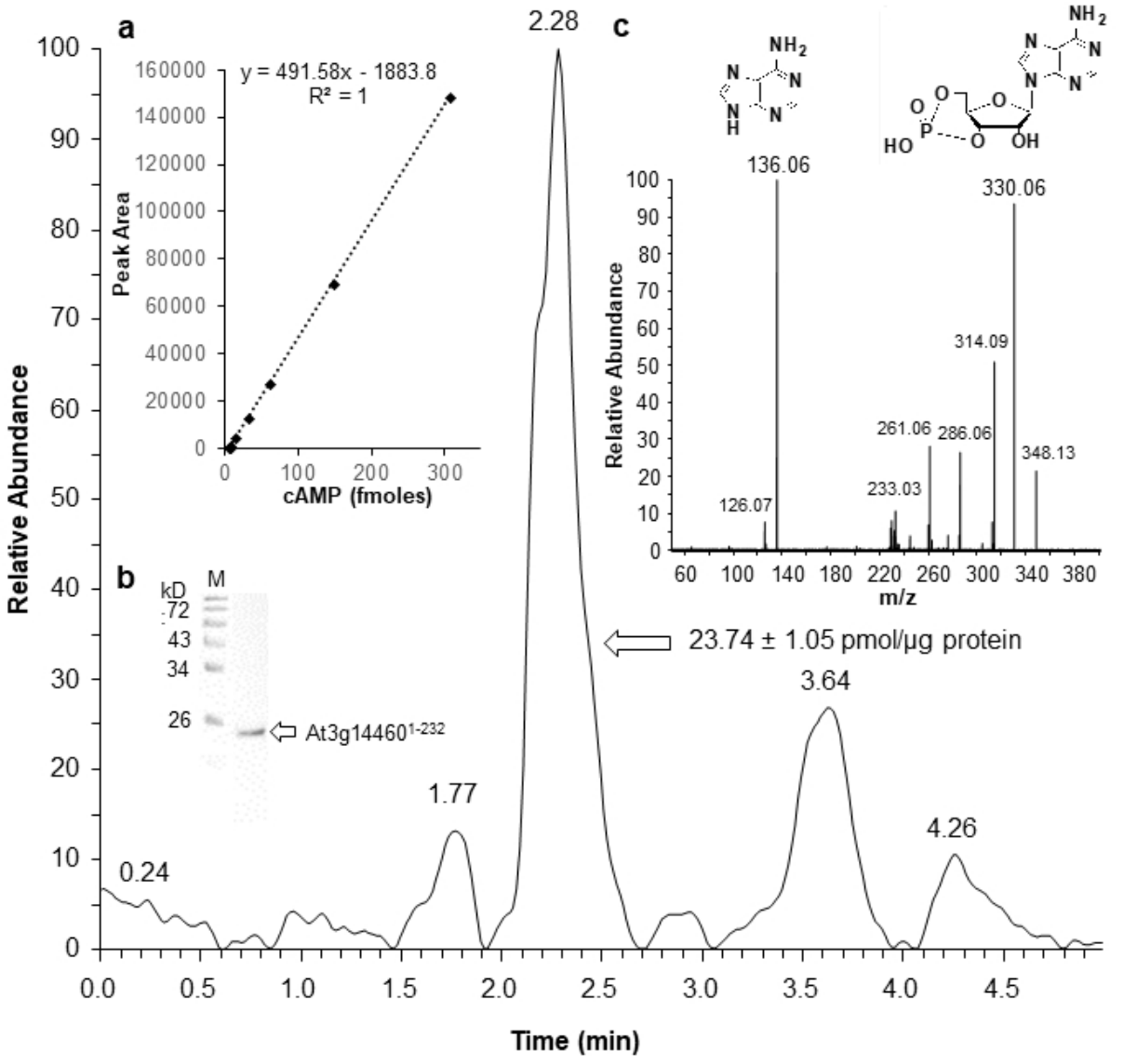
a
y = 491.58x - 1883.8
R² = 1
Peak Area
cAMP (fmoles)
b
kD
M
72
43
34
26
At3g14460 1-232
c
136.06
330.06
314.09
261.06
286.06
348.13
233.03
126.07
Relative Abundance
m/z
2.28
23.74 ± 1.05 pmol/µg protein
3.64
1.77
4.26
0.24
Relative Abundance
Time (min)

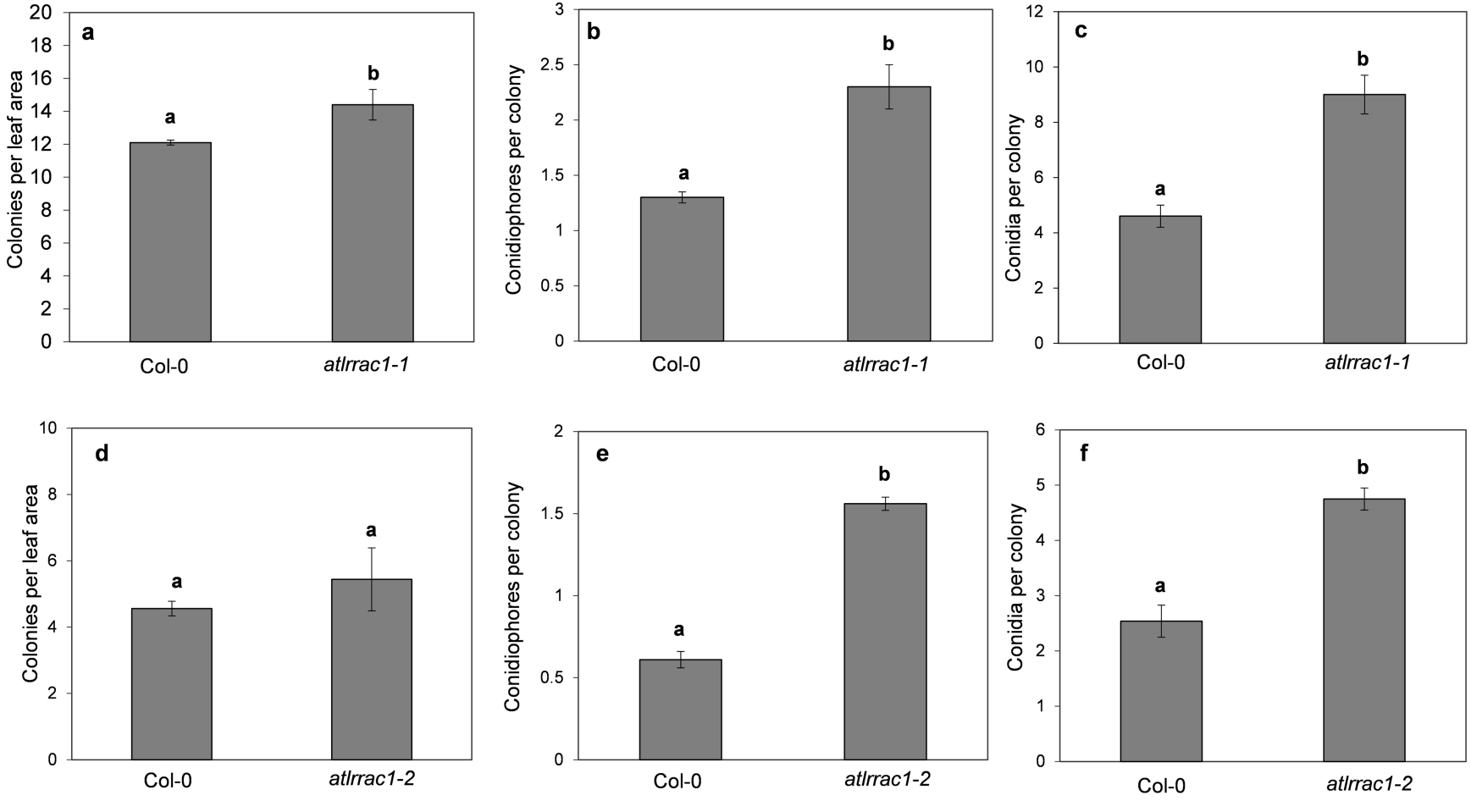
a
Colonies per leaf area
20
18
16
14
12
10
8
6
4
2
0
a
b
Col-0
atlrrac1-1
b
Conidiophores per colony
3
2.5
2
1.5
1
0.5
0
a
b
Col-0
atlrrac1-1
c
Conidia per colony
12
10
8
6
4
2
0
a
b
Col-0
atlrrac1-1
d
Colonies per leaf area
10
8
6
4
2
0
a
a
Col-0
atlrrac1-2
e
Conidiophores per colony
2
1.5
1
0.5
0
a
b
Col-0
atlrrac1-2
f
Conidia per colony
6
5
4
3
2
1
0
a
b
Col-0
atlrrac1-2

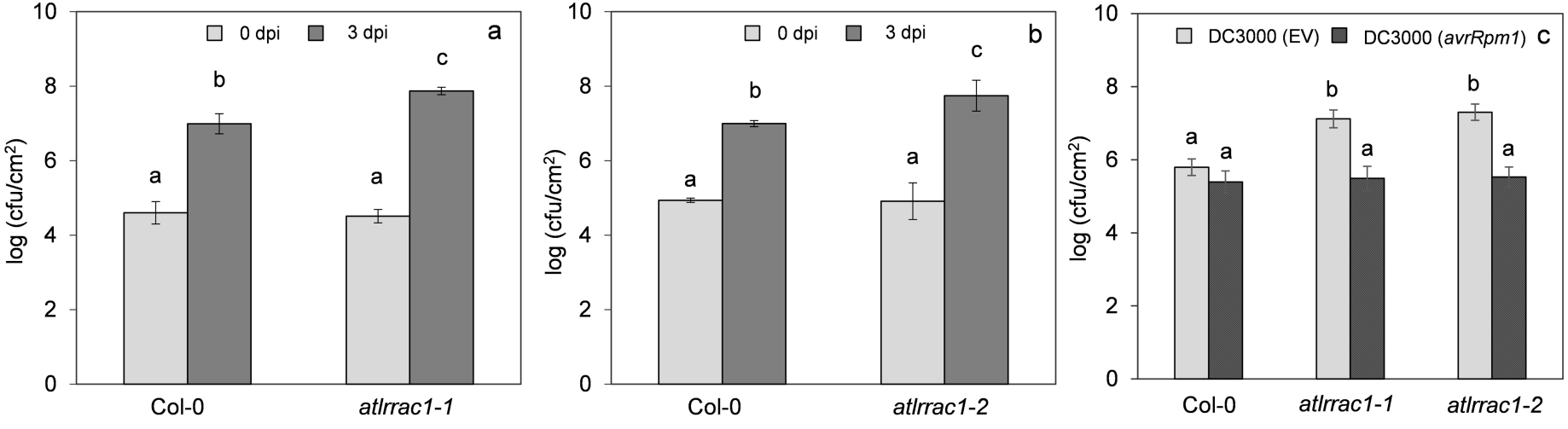
10
8
6
4
2
0
log (cfu/cm2)
0 dpi
3 dpi
a
b
c
a
a
Col-0
atlrrac1-1
10
8
6
4
2
0
log (cfu/cm2)
0 dpi
3 dpi
b
a
b
c
a
Col-0
atlrrac1-2
10
8
6
4
2
0
log (cfu/cm2)
DC3000 (EV)
DC3000 (avrRpm1)
c
a
a
b
a
b
a
Col-0
atlrrac1-1
atlrrac1-2

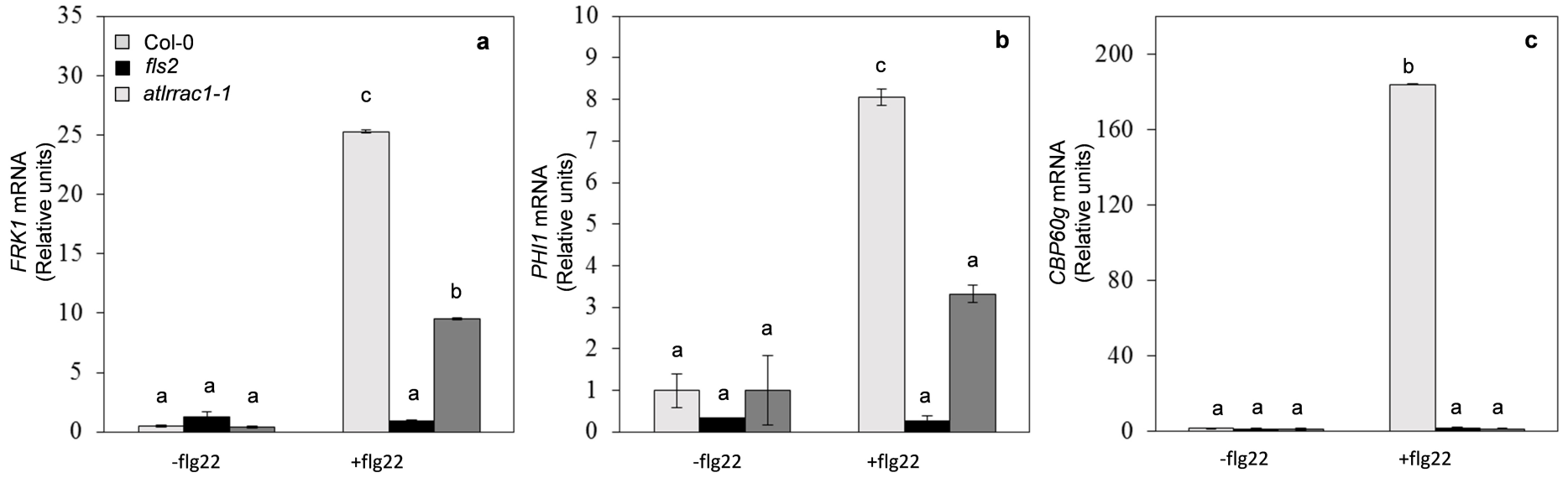
Col-0
fls2
atlrrac1-1
a
FRK1 mRNA (Relative units)
35
30
25
20
15
10
5
0
a a a c a b
-flg22
+flg22
b
PHI1 mRNA (Relative units)
10
9
8
7
6
5
4
3
2
1
0
a a a c a a
-flg22
+flg22
c
CBP60g mRNA (Relative units)
200
160
120
80
40
0
a a a b a a
-flg22
+flg22

Supplemental materials

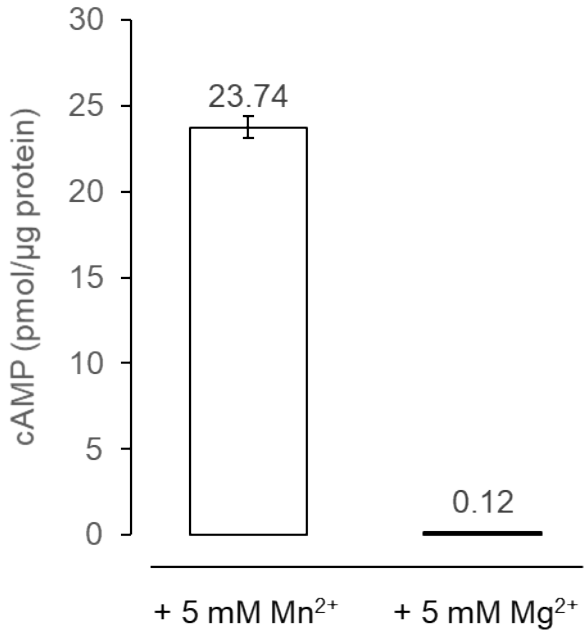

Figure S1. Detection of cAMP in reaction mixtures containing different cofactors by liquid chromatography tandem mass spectrometry (LC-MS/MS).
cAMP was generated from a reaction mixture containing 10 µg of affinity purified At3g14460$^{1-232}$ recombinant protein, 50 mM Tris-Cl; 2 mM IBMX, 1 mM ATP and 5 mM $MnCl_2$ or $MgCl_2$ cofactor. The amount of cAMP after 25 min of enzymatic reaction was determined to be 23.74 ± 1.05 pmol/µg protein and 0.12 ± 0.05 pmol/µg protein (n = 3) in the presence of Mn^{2+} and Mg^{2+} cofactor respectively.

RNA isolation and analysis of AtLRRAC1 transcript

Total RNA was extracted as reported in M&M section (*Flagellin (flg22) treatment and analysis of transcripts of immune-related genes*). For semiquantitative RT-PCR, 2 µg total RNA was reverse transcribed for 50 min at 42 °C using 200 U Superscript II reverse transcriptase (Invitrogen, Carlsbad, CA, USA) with 1× corresponding buffer, 10 mM dithiothreitol, 0.4 mM each dNTP, 0.5 µg oligo(dT)12–18 primer (Invitrogen). The cDNA was used for PCR with DreamTaq Green PCR Master Mix 1 U (Thermo Scientific, Waltha, Usa), 1× corresponding buffer, 0.2 mM each dNTP and 10 µM of primers (Invitrogen) (Table S1).

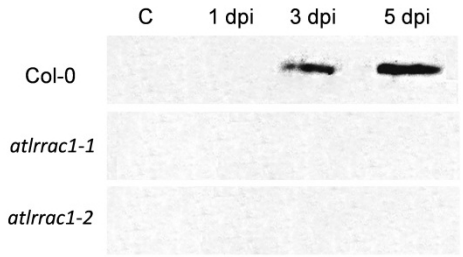

Figure S2. ***Quantification of*** *AtLRRAC1* ***transcripts in Arabidopsis Col-0*** **and mutant lines** ***(atlrrac1-1 and atlrrac1-2) inoculated with G. orontii.***

Quantification of *AtLRRAC1* mRNA was performed in uninoculated control plant (C) and at 1, 3 and 5 dpi after *G. orontii* inoculation. Total RNA was reverse transcribed and amplified by RT-PCR. Semi-quantification of mRNA levels loaded in each lane was performed by co-amplification and normalization with an internal standard (*EF-1α*).

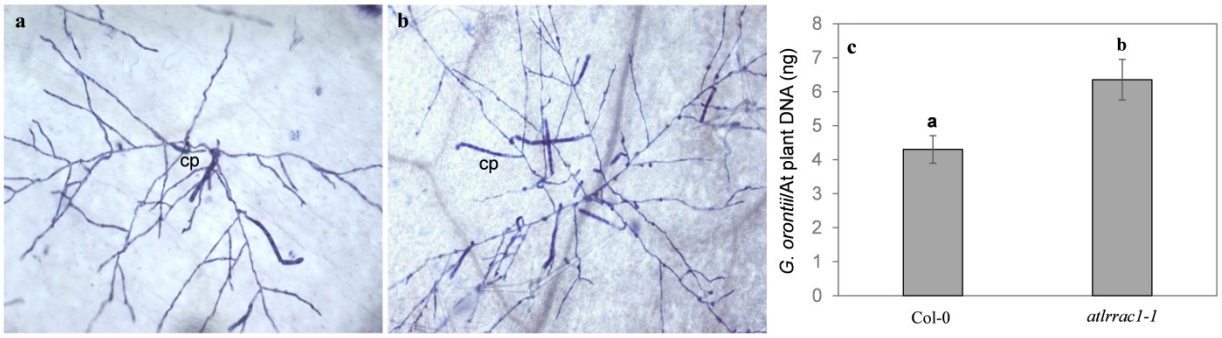

Figure S3. Quantification of infection levels on *atlrrac1-1* plants inoculated with *G. orontii*.
Representative Trypan blue-stained *G. orontii* colonies on Col-0 (a) and *atlrrac1-1* (b) Arabidopsis plants at 5 dpi. Cp indicates conidiophores and the scale bars are 100 μm. Genomic DNA quantification (b) by qPCR of *G. orontii* in pathogen inoculated Col-0 and *atlrrac1-1* plants was performed at 5 dpi. *G. orontii* biomass was expressed as the ratio between fungal and plant DNA. Amplification was performed using specific primers for *G. orontii* (*GDSL-like lipase*) and for Arabidopsis (*EF-1α* and *Act2),* as reported in Table S1. qPCR analysis was performed three times with three technical and three biological replicates (6 leaves each). Data are means ±SE, that were subject to one-way (genotype) analysis of variance (ANOVA) and compared by Tukey's HSD test.

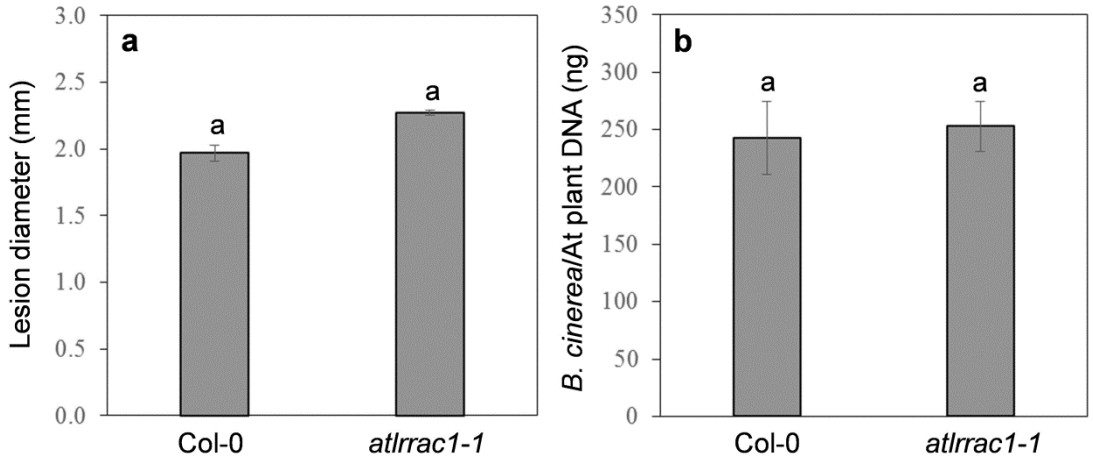

Figure S4. Pathogen growth quantification in *B. cinerea* inoculated Arabidopsis *Col-0* and *atlrrac1-1* plants.

Quantification of lesion diameter (a) in Arabidopsis plants inoculated with *B. cinerea* at 5 dpi. Data that are the means ±SE of three independent experiments were subject to one-way (genotype) analysis of variance (ANOVA) and Tukey's HSD test. In each experimnt, 24 leaves per genotype were drop inoculated in two points, for a total of 42 lesions. Quantification of pathogen by qRT-PCR (b) in Arabidopsis plants inoculated with *B. cinerea* at 5 dpi. *B. cinerea* biomass was expressed as the ratio between fungal and plant DNA. Amplification was performed using specific primers for *B. cinerea* (*DNA-dependent RNA polymerase subunit II*) and for Arabidopsis (*EF-1α* and *Act2),* as reported in Table S1. qRT-PCR analysis was performed three times with three technical and three biological replicates (6 leaves each). Data, expressed as means ±SE were subject to one-way (genotype) analysis of variance (ANOVA) and Tukey's HSD test.

Table S1. Oligonucleotide primer sequences and amplicon size (bp) used for DNA (fungal and plant) quantification and gene expression analysis by semi-quantitative and quantitative PCR.

Gene target	Primer	Sequence 5'-3'	Amplicon (bp)
Arabidopsis thaliana			
Leucine-rich repeat adenylyl cyclase 1 (At3g14460)	AtLRRAC1 fw	AATGCATTGAGTGGCCTACG	1142
	AtLRRAC1 bw	TGGCTGAGCACTGGTACTTG	
Elongation factor-1α (At1g07940)	EF-1α fw	AAGGAGGCTGCTGAGATGAA	120
	EF-1α bw	TGGTGGTCTCGAACTTCCAG	
Actin2 (At3g18780)	Act2 fw	AATCACAGCACTTGCACCA	99
	Act2 bw	GAGGGAAGCAAGAATGGAAC	
Tubulin Alpha-4 (At1g04820)	Tubα–4 fw	TACACCAACCTCAACCGCCT	152
	Tubα–4 bw	TGGGGCATAGGAGGAAAGCA	
FLG22-Induced Receptor-Like Kinase1 (At2g19190)	FRK1 fw	TGCAGCGCAAGGACTAGAG	107
	FRK1 bw	ATCTTCGCTTGGAGCTTCTC	
Calmodulin binding protein 60-like G(At5g2692)	CBP60g fw	AAGAAGAATTGTCCGAGAGGAG	129
	CBP60g bw	GGCGAGTTTATGAAGCACAG	
Phosphate-Induced 1 (At1g35140)	PHI1 fw	TTGGTTTAGACGGGATGGTG	134
	PHI1 bw	ACTCCAGTACAAGCCGATCC	
Golovinomyces orontii			
GDSL-like lipase	R263 fw	TCTTGGTGGCACGAATGAC	92
	R264 bw	AGTGCGAGAGTGGGACAGAC	
Botrytis cinerea			
DNA-dependent RNA polymerase subunit II	RPB2 fw	CGGCGCAAATGAGAAAGTGTG	149
	RPB2 bw	GTGAAATCAACAACAATCACC	